International Journal of Advanced Engineering and Technology Research
ISSN: 3106-8677 (Print), ISSN: 3106-8685 (Online) | Vol. 2, No. 1, 2026

Experimental Study of Droplet Impact on Superhydrophobic Surface at Different Speeds

Yanlong Zhao, Xinmin Zhang *

School of Mechanical and Power Engineering, Henan Polytechnic University, Jiaozuo 454003, PR China

* **Corresponding author**: (Email: zhangxinmin@hpu.edu.cn)

Abstract: The formation of ice caused by droplets hitting the cold surface may adversely affect the operation of various mechanical devices, causing a series of safety hazards. The surface modification with superhydrophobic properties effectively reduces the contact time and the heat exchange between the contact droplets and the cold surface, promotes the rapid shedding of droplets, and reduces the damage caused by the formation of ice layer. However, the research on the dynamics and heat tran sfer process of the effect of droplets on low-temperature superhydrophobic surfaces is still limited. The dynamic process of droplets with different Weber numbers impacting on different normal temperature surfaces was studied by using the prepared sample surface F1 ~ F5 and the visual droplet impact test bench. The experimental results show that the droplet spreading stage shows different dynamic characteristics with the change of droplet velocity and surface microstructure spacing. The microstructure spacing has little effect on the dynamic state of the impact droplet rebound with low Weber number, and mainly affects the dynamic state of the impact droplet rebound with high Weber number. The droplet spreading factor increases first and then decreases with the impact time, and is not affected by the surface microstructure spacing at lower Weber numbers. With the increase of Weber number and surface microstructure spacing, the variation curve of droplet spreading factor in the retractio n stage will be different. The maximum spreading factor of the droplet is directly affected by the Weber number, and there is a certain fitting relationship with the Weber number: $\beta_{max}=We^{1/4}$. The increase of surface microstructure spacing under high Weber number will make the change trend of max deviate from the fitting curve. Under the same surface, the droplet contact time Tc basically decreases with the increase of Weber number, while under the same Weber number, the change of microstructure spacing will cause the change of wetting state, so the droplet contact time basically decreases first and then increases. Thr ough energy analysis and statistics of the first rebound height of droplets, it is shown that with the change of Weber number and surface microstructure spacing, the change of droplet rebound height is opposite to the change trend of contact time. However, when Weber number is greater than a certain value, the change trend of dropl et rebound height is no longer corresponding to the change trend of droplet contact time, and the rebound height is generally reduced.

Keywords: Superhydrophobic surface, droplet impact, microstructure spacing, wetting state, contact time.

1. Introduction

The icing phenomenon of droplets impacting solid walls is widespread in the fields of cryogenic refrigeration, transmission, communication and aerospace. Impulsive droplets can cause great harm if they cannot be removed in time after icing. For example, in the field of low-temperature refrigeration, the impact of raindrops on the ice of outdoor heat exchangers will increase the thermal resistance and airflow resistance of heat exchangers and reduce heat transfer performance [1]. In the aerospace field, when the aircraft passes through the clouds, some supercooled water droplets in the clouds will hit the aircraft wings, engine inlets, propeller blades and other parts of the ice and easily cause the aircraft to crash out of control. [2, 3] In the field of energy and electricity, raindrops hitting wind turbine blades and icing can cause the wind turbine to stop running and reduce the fatigue life of the blades. [4] In the field of communication, under continuous rain and snow weather, freezing rain often freezes on the line and causes large-scale damage to the power grid after hitting the communication or transmission line, resulting in serious economic losses [5]. In the field of production and life, the freezing of raindrops hitting mechanical equipment often leads to reduced production efficiency or even stop production. The icing formed by droplet impact often causes catastrophic accidents and brings huge losses to human life and property. Therefore, it is of great significance to suppress the freezing of impinging droplets and study the corresponding anti-icing / de-icing technology.

The research on anti-icing / de-icing technology can be traced back to the last century. The use of certain measures to make supercooled water droplets fall off from the surface or cannot condense into ice before freezing is called anti-icing, and the removal of frozen ice is called de-icing. At present, there are two main anti-icing / de-icing methods used at home and abroad, namely active de-icing and passive anti-icing. Active de-icing is mainly divided into physical method and chemical method [6]. Physical de-icing refers to breaking the ice layer by applying external force to the ice layer manually or by means of some mechanical equipment, or melting the ice layer by means of the heat provided by the external heat source. Chemical de-icing refers to the spraying of substances such as deicing fluid or brine to reduce the temperature required for droplet freezing to dissolve the ice layer and prevent secondary icing. Passive anti-icing refers to the use of some anti-icing coatings to reduce the freezing point of water or reduce the adhesion of ice to the substrate to avoid the formation of ice or make the icing fall off naturally under wind and other conditions.

Although the traditional anti / de-icing technology has a certain effect, it is mostly based on the consideration of de-icing and melting ice. After the droplets freeze to form an ice layer, the ice layer is removed by physical or chemical methods. It does not consider preventing the impact droplets from freezing from the source and has many problems such as incomplete de-icing [7], waste of energy, and pollution of the environment [8]. Although passive anti-icing involves suppressing the freezing of impinging droplets from the source, the chemicals in the anti-icing coatings used in it have problems such as endangering human health [9] and destroying equipment performance [10]. These methods deviate from the concept of sustainable development such as 'green environmental protection, high efficiency and energy saving'. Therefore, it is an urgent problem to realize the anti-icing method with small energy consumption, high efficiency, green environmental protection and long-term stability. Animals and plants in nature have formed a unique biological mechanism after a long period of evolution. 'Growing silt without dyeing, cleaning the lian without demon' shows the self-cleaning effect on the surface of lotus leaves. In 1977, German scholars first revealed the unique wetting mechanism of lotus leaf surface and proposed the 'lotus leaf effect' [11]. They found that there were many micron-sized mastoid structures and protrusions wrapped with paraffin crystals on the surface of lotus leaf, which together achieved self-cleaning of lotus leaf surface. After that, Chinese academician Jiang Lei further found that there were many nano-scale particle structures distributed on the micron-scale mastoid structure on the surface of lotus leaf [12], which made the water droplets show a great contact angle and a small rolling angle on the surface of lotus leaf. Feng et al. [13] found that the surface of red rose petals has closely arranged micron-sized protrusions and stacked nanoparticles. These hierarchical micro / nanostructures provide sufficient roughness for the surface of the petals, so that the water droplets remain spherical on the surface of the petals and have a high adhesion force with the petals. Even if the petals are inverted, the water droplets cannot roll off. They define this phenomenon as 'petal effect'. In addition, scholars have also found similar unique wettability on peach skin [14], gecko foot hair [15], water strider [16], spider web and other organisms [17, 18].

A large number of studies have shown that the contact time between the impact droplet and the solid surface determines the degree of mass, momentum and heat transfer during the impact process [19, 20]. Shortening the contact time can minimize the energy exchange between the droplet and the surface, which is crucial for reducing heat transfer and improving anti-icing performance. Hu et al. [21] comprehensively discussed various methods to reduce the contact time of droplets, among which the superhydrophobic micropillar surface is considered to be one of the most effective designs. [22]. In this structure, the liquid penetrating the micro-pillar gap is rapidly discharged due to the capillary force, resulting in additional lift. This allows the droplets to quickly rebound from the surface of the micropillar to form a pancake-like shape. This phenomenon is called ' pancake rebound ', which shortens the contact time of the droplets by about 80 % [23, 24]. The latest research also emphasizes that the contact area is another key factor affecting the heat transfer of the droplet impact surface. Xiao et al. [25] observed that the microstructure of the superhydrophobic surface will capture a large amount of air. When the droplets contact the surface, the prominent tip of the micro-nano structure makes the droplets show a large contact angle, reducing the contact angle hysteresis, thereby reducing the contact area between the droplets and the surface, thereby reducing heat transfer.

In our experimental study, the dynamic process of droplet impact on low-temperature superhydrophobic surface was comprehensively studied. The dynamics and contact time changes of 2 mm droplets impacting superhydrophobic cold surfaces at − 15 ° C were studied. These surfaces have different microstructural spacings (ranging from 40 to 800μm). The change of droplet morphology was also analyzed. Based on the experimental results, the wetting transition mechanism of droplets under low temperature conditions is clarified, which provides valuable guidance for the development of anti-icing technology, especially in the de-icing of mechanical equipment in cold environment.

2. Experimental Method and Data Processing

2.1. Experimental Method

In this paper, the experimental study of droplets with different speeds or different scales impacting on superhydrophobic surfaces with different microstructure spacing is carried out by a self-built visual experimental device. During the experiment, the dynamic behavior of the droplet after impacting the superhydrophobic surface was recorded, and the effects of droplet velocity, droplet size and surface microstructure spacing on droplet contact time and wetting state were analyzed. Through the four subsystems of the visual experimental device, the precise control of factors such as droplet size, droplet velocity, surface temperature and environmental temperature and humidity is realized. The data image acquisition system is used to collect, store and process the experimental image data. The specific experimental steps are as follows:

Before the experiment, the experimental system device is checked to ensure that each experimental instrument can operate normally. The horizontal correction of the surface part is carried out by using the biaxial electronic level to ensure the accuracy of the experimental results. The model of the dual-axis electronic level is DXL360, and its accuracy is 0.1 °. The correction results are shown in Figure 2-9. The lower surface of the copper plate and the upper surface of the water-cooled row coated with thermally conductive silicone grease are tightly pressed together, and then the sample surface is placed on the upper surface of the copper plate. The thermally conductive silicone grease is applied between the two and the thermocouple is evenly arranged. In order to obtain accurate experimental temperature, thermocouples are also arranged around the surface to regulate the ambient temperature. Calculate the height of the free fall of the droplet according to the impact velocity of the droplet during the experiment, and then debug the droplet generator to ensure that it can drip normally. The high-speed camera shooting software on the computer is used for trial shooting. During the trial shooting process, the parameters such as the position, focal length, resolution, shooting frame rate and exposure time of the high-speed camera are adjusted to ensure that the integrity and clarity of the captured picture meet the requirements. In this process, it is also necessary to use the calibration caliper to record the image pixel ratio, so as to facilitate the subsequent data processing and the accuracy of data processing. Nitrogen is introduced into the organic glass box to remove the water vapor of the air to ensure that the environmental humidity meets the experimental requirements, and to avoid the frosting of water vapor at low temperatures affecting the experimental results. Turn on the low-temperature coolant circulating pump switch, through the T-type thermocouple, small fan and water cooling row and other equipment to monitor and adjust the temperature of the organic box to meet the experimental requirements. Open the thermostatic water bath and thermostat switch, set the thermostatic water bath temperature to 5 °C, and the preset temperature of the thermostat is adjusted to the surface temperature required for the experiment. Turn on the semiconductor 's DC power switch, the semiconductor refrigeration piece begins to continuously provide cooling to the sample surface, and the temperature controller monitors the real-time temperature of the surface to reach the preset temperature value and maintains its stability through relay interruption. Open the droplet generator to start the droplet, at the same time, open the high-speed camera and adjust it to the post-trigger mode to shoot, record the entire process of the droplet impact for subsequent data processing. In order to eliminate the influence of the error caused by the contingency of the experiment, each group of experiments was repeated at least three times, and the average value was taken as the experimental result to ensure the accuracy of the experimental results. After the experiment, the surface of the sample was removed for cleaning and all experimental equipment was closed.

3. Results and Analysis

3.1. Spreading and Rebounding Characteristics of Droplets

After the droplet impacts the superhydrophobic surface, it will produce different dynamic behaviors due to the influence of droplet characteristics and surface characteristics: spreading, retraction, rebound, splashing, deposition and so on. In order to explore the influence of droplet velocity and surface microstructure spacing on the droplet impact process, the droplet impact visualization experiment was carried out through the sample surface F1 ~ F5 under the condition that the experimental ambient temperature and surface temperature are both room temperature. The droplet diameter used in the experiment was 2.0 ± 0.05 mm. The impact velocities were 0.5 m / s, 1.0 m / s, 1.2 m / s, 1.4 m / s, 1.8 m / s and 2.2 m / s, respectively. The corresponding Weber numbers were We = 6.85, 27.40, 39.45, 53.70, 88.77 and 132.60, respectively. The whole experimental process was captured by a high-speed camera with a macro lens, and the dynamic state of the droplet when it reached the maximum spreading and the first rebound was recorded, as shown in Fig.1and Fig.2.

For droplet spreading, droplets exhibit different dynamic behaviors with the change of velocity and surface microstructure spacing. For the droplet with We = 6.85, due to the small droplet velocity, the droplet cannot be fully spread. As the kinetic energy of the droplet is completely converted into surface energy, the droplet as a whole is circular and has protrusions at the top. With the increase of the spacing of the microstructures, the protrusions at the top of the droplet gradually decrease, which is caused by the increase of the droplet sink caused by the increase of the spacing. As the Weber number of the droplet increases (We = 27.40), the kinetic energy of the droplet increases, the converted surface energy increases, and the degree of droplet spreading increases. At this time, the droplet exhibits a flat liquid ring. When the Weber number increases to 39.45, the dynamic behavior of the droplet is the same as before. The difference is that the top edge of the droplet on the F5 surface is no longer flat, showing a serrated shape. This phenomenon can also be observed on the surface of F1 at We = 53.70 and We = 88.77 and We = 132.60, and the serrated phenomenon is more obvious. This is because as the droplet hits the superhydrophobic surface with a high Weber number, the three-wire contact line at the edge of the droplet changes very quickly. When it spreads outward, it will carry some air into the droplet, resulting in uneven change rate of the three-phase contact line. The serrated shape will appear at the edge of the droplet and gradually form a liquid finger. The larger the Weber number is, the more air is encased when the droplet three-phase contact line is spread, and the more obvious the phenomenon is.

When the droplet impacts at a high Weber number, with the change of the microstructure spacing of the superhydrophobic surface, the dynamic state of the droplet is also different. For We = 88.77, the droplet shows the dynamic phenomenon of liquid finger breaking to form sub-droplet. This is because the droplet will instantaneously enter the retraction state after reaching the maximum spreading degree. At this time, the surface tension in the middle of the droplet is large, and the retraction speed of the central droplet is also greater than the retraction speed of the edge liquid finger, resulting in the phenomenon of wire drawing between the central main droplet and the liquid finger, and finally the liquid finger gradually breaks to form a secondary droplet. With the increase of the surface spacing of the sample, the number of secondary droplets gradually increases. This is because the larger the surface microstructure spacing, the smaller the resistance dissipation during the droplet spreading process, the greater the surface tension of the central droplet at the beginning of retraction, the faster the retraction will be, and the number of liquid finger breakage will increase. When the droplet hits the super-hydrophobic surface at We = 132.60, the droplet spreads rapidly under the condition of high-speed impact. The three-phase contact line of the droplet may be pinned in the microstructure with the increase of the surface microstructure spacing. Due to the Rayleigh-Plateau instability, the droplet will be truncated and broken to form independent small droplets and splash. In summary, the droplet velocity and surface microstructure spacing have a significant effect on the droplet impact process.

When the droplet impacts at a high Weber number, with the change of the microstructure spacing of the superhydrophobic surface, the dynamic state of the droplet is also different. For We = 88.77, the droplet shows the dynamic phenomenon of liquid finger breaking to form sub-droplet. This is because the droplet will instantaneously enter the retraction state after reaching the maximum spreading degree. At this time, the surface tension in the middle of the droplet is large, and the retraction speed of the central droplet is also greater than the retraction speed of the edge liquid finger, resulting in the phenomenon of wire drawing between the central main droplet and the liquid finger, and finally the liquid finger gradually breaks to form a secondary droplet. With the increase of the surface spacing of the sample, the number of secondary droplets gradually increases. This is because the larger the surface microstructure spacing, the smaller the resistance dissipation during the droplet spreading process, the greater the surface tension of the central droplet at the beginning of retraction, the faster the retraction will be, and the number of liquid finger breakage will increase. When the droplet hits the super-hydrophobic surface at We = 132.60, the

droplet spreads rapidly under the condition of high-speed impact. The three-phase contact line of the droplet may be pinned in the microstructure with the increase of the surface microstructure spacing. Due to the Rayleigh-Plateau instability, the droplet will be truncated and broken to form independent small droplets and splash. In summary, the droplet velocity and surface microstructure spacing have a significant effect on the droplet impact process.

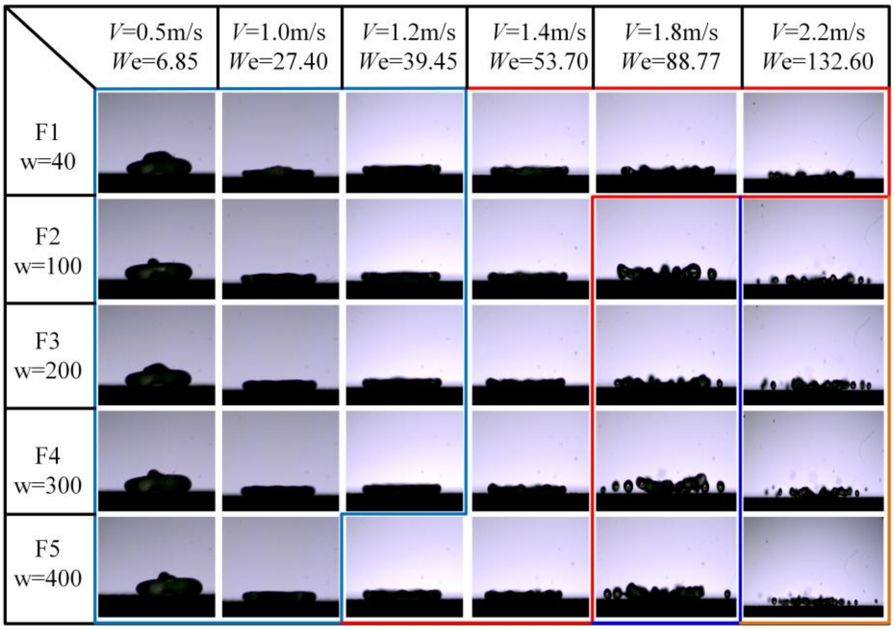

Figure 1. Dynamic characteristics of maximum droplet spreading

For droplet rebound, with the change of Weber number and surface microstructure spacing, the dynamic state of droplet rebound shows little difference. It is mainly reflected in the change of the overall length of the droplet rebound, that is, with the change of Weber number, it shows a trend of increasing first and then decreasing. This is indirectly caused by the change of surface energy. The larger the Weber number is, the more surface energy the droplet kinetic energy is converted into. Under the action of surface tension, the length of the droplet that gathers together and extends upward through the retraction process increases. As the Weber number continues to increase, the formation of secondary droplets and the splashing of small droplets will cause the surface energy of the main droplet to decrease, and the stretching length of the droplet rebound will decrease. Due to the change of the surface energy of the main droplet and the change of the microstructure spacing, the resistance of the droplet retraction and rebound is different, and the shape of the rebound is different. It can be seen that the microstructure spacing has little effect on the dynamic state of the low Weber number impinging droplet rebound, and mainly affects the dynamic state of the high Weber number impinging droplet rebound.

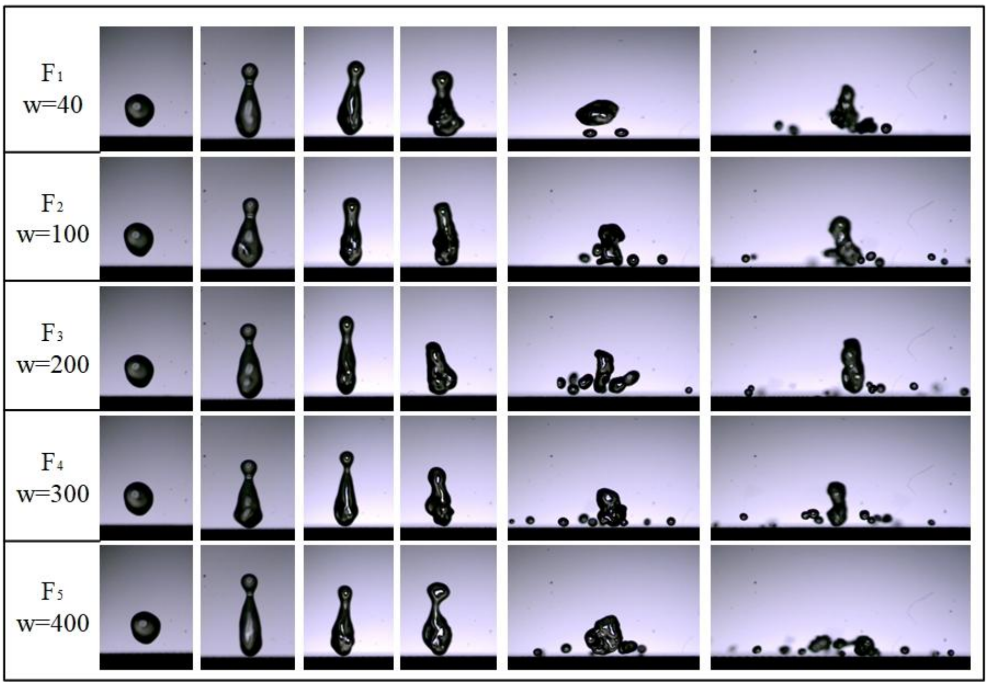

Figure 2. Dynamic characteristics of droplets rebounding

When the droplet breaks to form a secondary droplet or droplet splashing occurs, it is worth noting whether the secondary droplet and the splashed small droplet can eventually bounce off the surface, which is crucial for the anti-icing application of the superhydrophobic surface. In this regard, this paper records whether the droplets and small droplets can be detached from the surface after the droplets hit different surfaces at We = 88.77 and We = 132.6, as shown in Fig.3. From the diagram, it can be found that when We = 88.77, there will be no secondary droplets and small droplets on the F1 surface due to the spreading and rebounding stages, so only the main droplets remain on the surface. On the F2 ~ F5 surface, there are eventually small droplets remaining except the main droplets. This is because the kinetic energy of the small droplets formed by the breakup is less than the barrier that needs to be overcome for detachment from the surface. If the kinetic energy of the separated small droplets is greater than the barrier that needs to be overcome for detachment from the surface, there will be no droplets remaining on the surface, which can be seen on the F1 ~ F3 surface at We = 132.6. However, when the barrier required to overcome the detachment of small droplets from the surface decreases with the increase of the surface microstructure spacing, there are still spattered small droplets or main droplets on the F4 and F5 surfaces. The above situation shows that for the detachment of secondary droplets and small droplets from the surface, the droplet impact velocity and the surface microstructure spacing are not the larger the better, and the anti-icing effect of the superhydrophobic surface needs to be considered comprehensively.

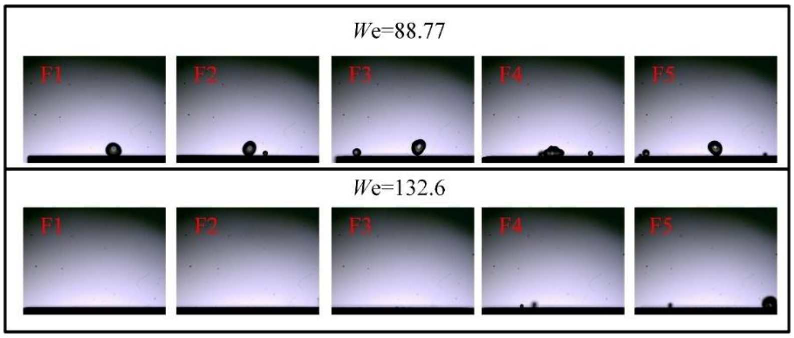

Figure 3. When We = 88.77 and We = 132.6, the residual state of droplets on the surface of F1 ~ F5 is

3.2. Droplet Spreading Factor

In order to better study the influence of droplet velocity and surface microstructure spacing on droplet impact process, the variation of droplet spreading factor on F1 ~ F5 surfaces with impact time under different Weber numbers was plotted, as shown in Fig. 4. At We = 88.77 and We = 132.60, the droplets will break and splash, and the droplet spreading factor cannot be counted. Therefore, this paper only draws the change of droplet spreading factor on different surfaces when We = 6.85 ~ 53.70. The droplet spreading factor is expressed as the ratio of the contact diameter between the droplet and the surface to the initial diameter of the droplet during the impact, denoted as 1 = D_1 / D_0 (D_1 is the contact diameter between the droplet and the surface, D0 is the initial diameter before the droplet impact).

It can be seen from the figure that the droplet spreading factor increases first and then decreases gradually to zero with time, and the change trend is not affected by droplet velocity and surface microstructure spacing. The droplet has not been in contact with the surface before the impact, and the droplet spreading factor is zero. When the droplet hits the superhydrophobic surface, the kinetic energy of the droplet is converted into surface energy, which tends to spread the droplet around. The contact diameter between the droplet and the surface increases, and the droplet spreading factor increases. When the droplet spreading degree reaches the maximum, the droplet spreading factor reaches the maximum. After that, the droplet begins to retract to the center under the action of surface tension, resulting in a decrease in the contact diameter of the droplet and a decrease in the droplet spreading factor. When the droplet bounces off the surface, the contact diameter between the droplet and the surface is zero, and the droplet spreading factor is zero, reaching the minimum. The change of the whole impact process can be seen in the small figure of We = 39.45.

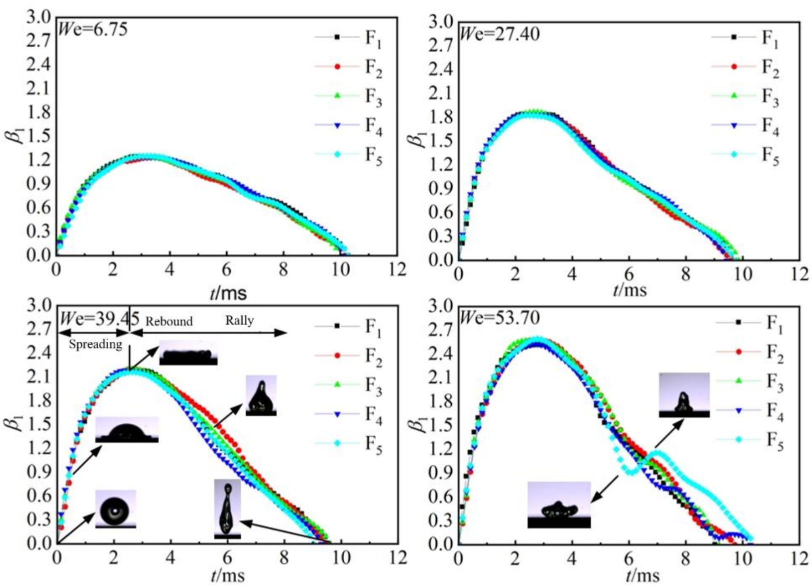

Figure 4. The variation curves of droplet spreading factor on F1 ~ F5 surfaces with time under different Weber numbers

As the Weber number increases from We = 6.75 to We = 53.70, the maximum spreading factor of droplets increases from about 1.2 to about 2.4, but the maximum spreading factors of droplets on F1 ~ F5 surfaces are basically the same at lower Weber numbers, indicating that the droplet spreading diameter is mainly affected by the droplet velocity, and the surface microstructure spacing has little effect on the droplet contact diameter. By comparing the spreading factor curves of the droplets on the F1 ~ F5 surfaces during the spreading process and the retraction process, it can be found that at a lower Weber number (We = 6.75), the curves of the droplet spreading factor in the spreading stage and the retraction stage are basically the same, and are not affected by the surface microstructure spacing. With the increase of Weber number (We = 39.45), the variation curve of droplet spreading factor in the retraction stage will be different. With the further increase of Weber number, the difference of spreading factor curve in the retraction stage of droplets on the surface with larger microstructure spacing will be more obvious, as shown on the surface of F3 and F4 when We = 53.70. This is because as the droplet Weber number and the surface microstructure spacing increase to a certain extent, the droplet will penetrate into the surface microstructure at a high Weber number, and the change of the surface microstructure spacing causes the difference in the resistance required to overcome the retraction process, resulting in a significant change in the change trend of the droplet contact diameter. As the surface microstructure spacing continues to increase, on the one hand, the droplets overcome different resistances to cause their retraction asymmetry ; on the other hand, when the droplets are pinned in the microstructure, a force will be generated on the depinned droplets, causing the bottom of the droplets to re-contact the surface of the sample, thereby increasing the droplet spreading factor (We = 53.70, F5), resulting in the spreading factor curve increasing first and then decreasing.

4. Conclusion

In this chapter, the dynamic process of droplets with different Weber numbers impacting on different normal temperature surfaces was studied by preparing the sample surface F1 ~ F5 with a visual droplet impact test bench. The experimental results show that: The droplet spreading stage shows different dynamic characteristics with the change of droplet velocity and surface microstructure spacing. The micro-structure spacing has little effect on the dynamic state of the impact droplet rebounding at low Weber number, but mainly affects the dynamic state of the impact droplet rebounding at high Weber number. The droplet spreading factor increases first and then decreases with the impact time, and is not affected by the surface microstructure spacing at lower Weber numbers. With the increase of Weber number and surface microstructure spacing, the variation curve of droplet spreading factor in the retraction stage will be different. The maximum spreading factor of the droplet is directly affected by the Weber number, and there is a certain fitting relationship with the Weber number: max = We1 / 4. The increase of surface microstructure spacing under high Weber number will make the change trend of max deviate from the fitting curve. Under the same surface, the droplet contact time Tc basically decreases with the increase of Weber number, while under the same Weber number, the droplet contact time basically decreases first and then increases due to the change of wetting state caused by the change of microstructure spacing. Through energy analysis and statistics of the first rebound height of droplets, it is shown that with the change of Weber number and surface microstructure spacing, the change of droplet rebound height is opposite to the change trend of contact time. However, when Weber number is greater than a certain value, the change trend of droplet rebound height is no longer corresponding to the change trend of droplet contact time, and the rebound height is generally reduced.

Acknowledgments

This work was financially supported by the National Science Foundation of China (No. 52266001), the Science and Technology Research Project of Henan Province (No. 232102241014), the Key scientific research project of Henan Province Colleges and Universities (No. 22A470002) and Doctoral Fund Project of Henan Polytechnic University (No. B2021-37).

References

[1] M. Tarfaoui, M. Nachtane, H. Khadimallah, D. Saifaoui, Simulation of mechanical behavior and damage of a large composite wind turbine blade under critical loads, Appl. Compos. Mater. 25 (2018) 237–254.

[2] O. Lagdani, M. Tarfaoui, M. Nachtane, M. Trihi, H. Laaouidi, Numerical investigation of ice accretion on an offshore composite wind turbine under critical loads, Int. J. Energy Res. 45 (2021) 4112–4132.

[3] H.U. Sajid, A. Jalal, R. Kiran, A. Al-Rahim, A survey on the effects of deicing materials on properties of Cement-based materials, Construction and Building Materials 319 (2022) 126062.

[4] X. Wei, J. Wei, Y. Feng, J. Wang, Photothermal hydrophobic coating with light-trapping and thermal isolated effects for efficient photothermal anti-icing/de-icing, Progress in Organic Coatings 179 (2023) 107550.

[5] L. Wu, P. Liu, X. Hua, Z. Guo, W. Liu, Photothermal superhydrophobic membrane based on breath figure: Anti-icing and deicing, Chemical Engineering Journal 480 (2024) 147553.

[6] E. Vazirinasab, R. Jafari, G. Momen, Application of superhydrophobic coatings as a corrosion barrier: A review, Surface and Coatings Technology 341 (2018) 40-56.

[7] A. Mohiley, J. Franzaring, O.C. Calvo, A. Fangmeier, Potential toxic effects of aircraft de-icers and wastewater samples containing these compounds, Environmental Science and Pollution Research 22(17) (2015) 13094-13101.

[8] W. Barthlott, C. Neinhuis, Purity of the sacred lotus, or escape from contamination in biological surfaces, Planta 202(1) (1997) 1-8.

[9] X. Lu, H. Cai, Y. Wu, C. Teng, C. Jiang, Y. Zhu, L. Jiang, Peach skin effect: a quasi-superhydrophobic state with high adhesive force, Science Bulletin 60(4) (2015) 453-459.

[10] K. Autumn, M. Sitti, Y.A. Liang, A.M. Peattie, W.R. Hansen, S. Sponberg, T.W. Kenny, R. Fearing, J.N. Israelachvili, R.J. Full, Evidence for van der Waals adhesion in gecko setae, Proceedings of the National Academy of Sciences 99(19) (2002) 12252-12256.

[11] X. Gao, L. Jiang, Biophysics: water-repellent legs of water striders, Nature 432(7013) (2004) 36.

[12] F. Gao, Y. Yao, W. Wang, X. Wang, L. Li, Q. Zhuang, S. Lin, Light-Driven Transformation of Bio-Inspired Superhydrophobic Structure via Reconfigurable PAzoMA

Microarrays: From Lotus Leaf to Rice Leaf, Macromolecules 51(7) (2018) 2742-2749.

[13] J. Ju, H. Bai, Y. Zheng, T. Zhao, R. Fang, L. Jiang, A multi-structural and multi-functional integrated fog collection system in cactus, Nature communications 3 (2012) 1247.

[14] H. Ning, T. Zhang, L.-Z. Zhang, Application of self-assembly methods in the preparation of superhydrophobic surfaces: A review, Surfaces and Interfaces 51 (2024) 104765.

[15] S. Hu, T. Reddyhoff, D. Puhan, S.-C. Vladescu, X. Shi, D. Dini, Z. Peng, Droplet manipulation of hierarchical steel surfaces using femtosecond laser fabrication, Applied Surface Science 521 (2020) 146474.

[16] C.-Y. Huang, M.-F. Lai, W.-L. Liu, Z.-H. Wei, Anisotropic Wettability of Biomimetic Micro/Nano Dual-Scale Inclined Cones Fabricated by Ferrofluid-Molding Method, Advanced Functional Materials 25(18) (2015) 2670-2676.

[17] L. Qian, B. Huo, Z. Chen, E. Li, H. Ding, Droplet bouncing on moving superhydrophobic groove surfaces, International Journal of Multiphase Flow 165 (2023) 104454.

[18] L. Ding, W. Liu, S. Dong, X. Li, Y. Yu, Z. Cui, L. An, Fabrication of robust superhydrophobic surface on TC4 alloy by wire electrical discharge machining, Journal of Alloys and Compounds 988 (2024) 174329.

[19] C. Shu, Q. Su, M. Li, Z. Wang, S. Yin, S. Huang, Fabrication of extreme wettability surface for controllable droplet manipulation over a wide temperature range, International Journal of Extreme Manufacturing 4(4) (2022) 045103.

[20] Y. Fan, Y. Tan, Y. Dou, S. Huang, X. Tian, Reducing the contact time of bouncing droplets on superhydrophobic surfaces: Foundations, strategies and applications, Chemical Engineering Journal 476 (2023) 146485.

[21] J. Du, Y. Li, X. Wu, Q. Min, Steerable directional bouncing and contact time reduction of impacting droplets on superhydrophobic stepped surfaces, Journal of Colloid and Interface Science 629 (2023) 1032-1044.

[22] Z. Hu, F. Chu, H. Shan, X. Wu, Z. Dong, R. Wang, Understanding and Utilizing Droplet Impact on Superhydrophobic Surfaces: Phenomena, Mechanisms, Regulations, Applications, and Beyond, Adv Mater 36(11) (2024) e2310177.

[23] Y. Liu, L. Moevius, X. Xu, T. Qian, J.M. Yeomans, Z. Wang, Pancake bouncing on superhydrophobic surfaces, Nature Physics 10(7) (2014) 515-519.

[24] L. Moevius, Y. Liu, Z. Wang, J.M. Yeomans, Pancake bouncing: simulations and theory and experimental verification, Langmuir 30(43) (2014) 13021-32.

[25] X. Yan, L. Zhang, S. Sett, L. Feng, C. Zhao, Z. Huang, H. Vahabi, A.K. Kota, F. Chen, N. Miljkovic, Droplet Jumping: Effects of Droplet Size, Surface Structure, Pinning, and Liquid Properties, ACS Nano 13(2) (2019) 1309-1323.